



HAL
open science

Deep sourced fluids for peridotite carbonation in the shallow mantle wedge of a fossil subduction zone: Sr and C isotope profiles of OmanDP Hole BT1B

Juan Carlos de Obeso, Peter B Kelemen, James M Leong, Manuel D Menzel, Craig E Manning, Marguerite Godard, Yue Cai, Louise Bolge

► To cite this version:

Juan Carlos de Obeso, Peter B Kelemen, James M Leong, Manuel D Menzel, Craig E Manning, et al.. Deep sourced fluids for peridotite carbonation in the shallow mantle wedge of a fossil subduction zone: Sr and C isotope profiles of OmanDP Hole BT1B. *Journal of Geophysical Research: Solid Earth*, 2022, 127 (1), pp.e2021JB022704. 10.1029/2021JB022704 . hal-03523083

HAL Id: hal-03523083

<https://hal.science/hal-03523083>

Submitted on 12 Jan 2022

HAL is a multi-disciplinary open access archive for the deposit and dissemination of scientific research documents, whether they are published or not. The documents may come from teaching and research institutions in France or abroad, or from public or private research centers.

L'archive ouverte pluridisciplinaire **HAL**, est destinée au dépôt et à la diffusion de documents scientifiques de niveau recherche, publiés ou non, émanant des établissements d'enseignement et de recherche français ou étrangers, des laboratoires publics ou privés.

1 **Deep sourced fluids for peridotite carbonation in the shallow mantle wedge of a fossil**
2 **subduction zone: Sr and C isotope profiles of OmanDP Hole BT1B**
3

4 **Juan Carlos de Obeso^{1,2}, Peter B. Kelemen², James M. Leong², Manuel D. Menzel³, Craig**
5 **E. Manning⁴, Marguerite Godard⁵, Yue Cai², Louise Bolge² and Oman Drilling Project**
6 **Phase 1 Science Party[†]**

7 ¹ Department of Geosciences, University of Calgary, Calgary, Canada

8 ² Lamont Doherty Earth Observatory, Columbia University, Palisades, NY, USA.

9 ³ Institute of Tectonics and Geodynamics, RWTH Aachen University, Aachen, Germany.

10 ⁴ Dept. of Earth & Space Sciences, University of California, Los Angeles, CA, USA.

11 ⁵ Géosciences Montpellier, Université de Montpellier, CNRS, Montpellier, France.

12

13 Corresponding author: Juan Carlos de Obeso (juancarlos.deobeso@ucalgary.ca) and Yue Cai
14 (merrycai@gmail.com)

15

16

17 **Key Points:**

- 18 • Strontium and Carbon were added to the peridotites during alteration of mantle peridotite
19 with carbonated fluid derived from decarbonation reaction.
20

- 21 †**Oman Drilling Project Phase 1 Science Party**
22 Jürg Matter, University of Southampton, United Kingdom
23 Damon Teagle, University of Southampton, United Kingdom
24 Jude Coggon, University of Southampton, United Kingdom
25 Michelle Harris, Plymouth University, United Kingdom
26 Emma Bennett, Cardiff University, United Kingdom
27 Nico Bompard, University of Southampton, United Kingdom
28 Marine Boulanger, Centre de Recherches Pétrographiques et Géochimiques, France
29 Lyderic France, Université de Lorraine, France
30 Gretchen Früh-Green, ETH Zurich, Switzerland
31 Dieter Garbe-Schönberg, Christian-Albrecht University of Kiel, Germany
32 Benoit Ildefonse, Université de Montpellier, France
33 Ana Jesus, German University of Technology in Oman, Oman
34 Jürgen Koepke, Leibniz University Hannover, Germany
35 Louise Koornneef, Plymouth University, United Kingdom
36 Romain Lafay, University of Lausanne, Switzerland
37 Johan Lissenberg, Cardiff University, United Kingdom
38 Chris MacLeod, Cardiff University, United Kingdom
39 Dominik Mock, Leibniz University of Hanover, Germany
40 Tony Morris, Plymouth University, United Kingdom
41 Samuel Müller, Kiel University, Germany
42 Julie Noël, Université de Montpellier, France
43 Daniel Nothaft, University of Colorado, USA
44 Americus Perez, Kanazawa University, Japan
45 Philippe Pezard, Université de Montpellier, France
46 Nehal Warsi, AZD Engineering, Oman
47 David Zeko, University of British Columbia, Canada
48 Barbara Zihlmann, University of Southampton, United Kingdom
49 Mohamed-Amine Bechkit, Houari Boumediene University, Algeria
50 Laurent Brun, University of Montpellier, France
51 Bernard Célrier, University of Montpellier, France
52 Gilles Henry, University of Montpellier, France
53 Jehanne Paris, University of Montpellier, France
54 Gérard Lods, University of Montpellier, France
55 Pascal Robert, Université de Lorraine, Nancy, France
56 Salim Al Amri, Ministry of Regional Municipalities and Water Resources, Sultanate of Oman
57 Mohsin Al Shukaili, Ministry of Regional Municipalities and Water Resource, Sultanate of Oman
58 Ali Al Qassabi, Ministry of Regional Municipalities and Water Resources, Sultanate of Oman
59 Kyaw Moe, Japan Agency for Marine-Earth Science and Technology (JAMSTEC), Japan
60 Yasu Yamada, Japan Agency for Marine-Earth Science and Technology (JAMSTEC), Japan
61 Eiichi Takazawa, Niigata University, Japan
62 Katsuyoshi Michibayashi, Shizuoka University, Japan
63 Natsue Abe, JAMSTEC, Japan
64 Tetsu Akitou, Okayama University, Japan
65 Salim Ahmed AlShahri, Public Authority for Mining, Oman
66 Hamood Hamed Shames Al-Siyabi, MRMWR, Oman

67 Saif Masoud Alhumaimi, Public Authority for Mining, Oman
68 Maqbool Hussein AlRawahi, MRMWR, Oman
69 Musaab Shaker Al Sarmi, Sultan Qaboos University, Oman
70 Bader Hamed Alwaeli, Sultan Qaboos University, Oman
71 Andreas Beinlich, University of Bergen, Norway
72 Elliot Carter, University of Manchester, United Kingdom
73 Mike Cheadle, University of Wyoming, USA
74 Mark Cloos, University of Texas at Austin, USA
75 Matthew Cooper, University of Southampton, United Kingdom
76 Laura Crispini, University of Genova, Italy
77 Joëlle D'Andres (was Ducommun), Australian National University, Australia
78 Luke Deamer, Cardiff University, United Kingdom
79 Jeremy Deans, University of Southern Mississippi, USA
80 Kathi Faak, Ruhr-Universitaet Bochum, Germany
81 Rebecca Greenberger, California Institute of Technology, USA
82 Yumiko Harigane, National Institute of Advanced Industrial Science and Technology, Japan
83 Kohei Hatakeyama, Hiroshima University, Japan
84 Andrew Horst, Marshall University, USA
85 Takashi Hoshide, Akita University, Japan
86 Keisuke Ishii, Niigata University, Japan
87 Kevin Johnson, University of Hawaii, USA
88 Michael Kettermann, Aachen University, Germany
89 Hogyum Kim, Seoul National University, Republic of Korea
90 Jürgen Koepke, Leibniz University Hannover, Germany
91 Kentaro Kondo, Akita University, Japan
92 Alissa Kotowski, University of Texas at Austin, USA
93 Fatna Kourim, Academia Sinica, Taiwan
94 Yuki Kusano, Geological Survey of Japan, Japan
95 Catriona Menzies, University of Southampton, United Kingdom
96 Tomoaki Morishita, Kanazawa University, Japan
97 Tony Morris, Plymouth University, United Kingdom
98 Du Khac Nguyen, Kanazawa University, Japan
99 Toshio Nozaka, Okayama University, Japan
100 Keishi Okazaki, JAMSTEC, Japan
101 Suzanne Picazo, University of Lausanne, Switzerland
102 Ryoko Senda, Kyushu University, Japan
103 Yamato Tateishi, Okayama University, Japan
104 Jessica Till, University of Iceland, Iceland
105 Susumu Umino, Kanazawa University, Japan
106 Janos Urai, Aachen University, Germany
107 Yoichi Usui, JAMSTEC, Japan
108
109

110 **Abstract**

111 Completely carbonated peridotites represent a window to study reactions of carbon-rich fluids
 112 with mantle rocks. Here we present details on the carbonation history of listvenites close to the
 113 basal thrust in the Samail ophiolite. We use samples from Oman Drilling Project Hole BT1B,
 114 which provides a continuous record of lithologic transitions, as well as outcrop samples from
 115 listvenites, metasediments and metamafics below the basal thrust of the ophiolite. $^{87}\text{Sr}/^{86}\text{Sr}$ of
 116 listvenites and serpentinites, ranging from 0.7090 to 0.7145, are significantly more radiogenic
 117 than mantle values, Cretaceous seawater, and other peridotite hosted carbonates in Oman. The
 118 Hawasina sediments that underlie the ophiolite, on the other hand, show higher $^{87}\text{Sr}/^{86}\text{Sr}$ values
 119 of up to 0.7241. $\delta^{13}\text{C}$ values of total carbon in the listvenites and serpentinites range from -
 120 10.6‰ to 1.92‰. We also identified a small organic carbon component with $\delta^{13}\text{C}$ as low as -
 121 27‰. Based on these results, we propose that during subduction at temperatures above $>400^\circ\text{C}$,
 122 carbon-rich fluids derived from decarbonation of the underlying sediments migrated updip and
 123 generated the radiogenic $^{87}\text{Sr}/^{86}\text{Sr}$ signature and the fractionated $\delta^{13}\text{C}$ values of the serpentinites
 124 and listvenites in core BT1B.

125

126 **Plain Language Summary**

127 Samples from Oman Drilling Project Hole BT1B provide a record of interactions of fluids rich in
 128 carbon dioxide with mantle rocks. This interactions lead to the formation of listvenites, rocks
 129 composed mainly by magnesite and quartz. Here we describe the formation of listvenites in the
 130 Oman ophiolite using Strontium and Carbon isotopes to characterize the source and nature of the
 131 fluid that pervasively transform the mantle rocks that now store vast amounts of carbon dioxide.

132 **1 Introduction**

133 Hydration and carbonation of ultramafic rocks are important processes in the carbon and
 134 water cycle of our planet (Alt et al., 2013; Fruh-Green et al., 2004). These alteration reactions are
 135 sinks of water and carbon where peridotites are exposed on the seafloor forming alteration
 136 minerals like serpentine and carbonates (Alt et al., 2013; Klein et al., 2020; Macdonald & Fyfe,
 137 1985; Paulick et al., 2006) which are carried back into the mantle in convergent margins. Fluids
 138 derived from the subducted slab can migrate and interact with the mantle wedge in subduction
 139 zones, so that the “leading edge of the mantle wedge” aka the “cold nose”, can be partially
 140 hydrated and carbonated (Blakely et al., 2005; Hyndman & Peacock, 2003; Kelemen &
 141 Manning, 2015). This is usually inferred from seismic data (e.g. DeShon and Schwartz, 2004;
 142 Kamiya and Kobayashi, 2000; Tibi et al., 2008; Tsuji et al., 2008). Understanding the interaction
 143 of carbon-bearing hydrous fluids with peridotites is important to supplement and constrain
 144 geophysical observations.

145

146 Fully carbonated peridotites, also known as listvenites (Halls & Zhao, 1995), provide a
 147 window into the alteration processes that occur in the “cold nose” of the mantle wedge above
 148 subduction zones, where mantle peridotite reacts with hydrous and carbonated fluids likely
 149 derived from the subducting slab at moderate temperatures and pressures (Beinlich et al., 2012;
 150 Boskabadi et al., 2017, 2020; Falk & Kelemen, 2015; Menzel et al., 2018). Formation of
 151 listvenites appears to be restricted to particular conditions requiring high carbon concentrations

152 in the fluid (Falk & Kelemen, 2015; Hansen et al., 2005; Kelemen et al., 2021; Menzel et al.,
 153 2018). For example, complete carbonation of peridotites to form listvenites is not observed near
 154 the surface in ophiolites (e.g. Clark and Fontes, 1990; de Obeso and Kelemen, 2020, 2018;
 155 Garcia del Real et al., 2016; Kelemen and Matter, 2008; Noël et al., 2018; Quesnel et al., 2016;
 156 Schwarzenbach et al., 2016). It is also not observed near the seafloor, where serpentinization and
 157 formation of carbonate veins are common (e.g. Bach et al., 2011; Delacour et al., 2008;
 158 Schwarzenbach et al., 2013). Fluid sources for complete carbonation have been associated with
 159 subduction in different listvenite localities. Menzel et al. (2018) attributed carbonation of
 160 harzburgite in the Advocate ophiolite (Canada) to fluxing by slab-derived, CO₂-rich fluids.
 161 Isotopic data ($\delta^{13}\text{C}$, $\delta^{18}\text{O}$ and $^{87}\text{Sr}/^{86}\text{Sr}$) of listvenites in the Late Cretaceous ophiolites of eastern
 162 Iran point to carbon-bearing fluids derived from subducted sedimentary units as the source of
 163 carbon (Boskabadi et al., 2020).

164 In Oman, listvenites occur along the basal thrust of the ophiolite (Nasir et al., 2007;
 165 Wilde et al., 2002). Previous studies have investigated their formation conditions and the nature
 166 of the carbonation fluids without reaching conclusive answers on the source of the fluids
 167 (Beinlich et al., 2020; Falk & Kelemen, 2015; Nasir et al., 2007; Stanger, 1985). In this paper,
 168 we present $^{87}\text{Sr}/^{86}\text{Sr}$ and $\delta^{13}\text{C}$ data on samples from Oman Drilling Project Hole BT1B and the
 169 underlying sediments of the Hawasina Formation. We show that devolatilization of the subducting
 170 sediments similar to the Hawasina Formation likely generated the carbonation fluids which
 171 reacted with the mantle wedge in this fossil subduction zone to form listvenites. These processes
 172 probably operate in subduction zones worldwide, where fluids migrate updip along the slab
 173 mantle interface, and then react with hanging wall peridotites storing large amounts of carbon.

174

175 **2 Geological setting**

176 *2.1 The Samail ophiolite*

177 The Samail ophiolite, along the northeast coast of Oman and the United Arab Emirates
 178 (UAE), is one of the best-exposed block of oceanic crust and its underlying mantle in the world.
 179 It was thrust over adjacent oceanic lithosphere soon after magmatic formation, and then onto the
 180 margin of the Arabian subcontinent in the late Cretaceous. The mantle section of the ophiolite is
 181 mainly composed of highly depleted, residual mantle peridotites (mostly harzburgites, e.g.
 182 (Godard et al., 2000; Hanghøj et al., 2010; Monnier et al., 2006), together with 5 to 15% dunite
 183 (Braun, 2004; Braun & Kelemen, 2002; Collier, 2012). Near the basal thrust, interlayered dunites
 184 and refertilized harzburgites comprise the distinctive “Banded Unit” (Khedr et al., 2014). The
 185 peridotites are pervasively serpentinized, with serpentine (\pm brucite) making up \sim 30-100 wt% of
 186 “fresh” rock (Godard et al., 2000; Hanghøj et al., 2010; Monnier et al., 2006) and/or completely
 187 carbonated to form listvenites (Falk & Kelemen, 2015; Nasir et al., 2007; Stanger, 1985; Wilde
 188 et al., 2002). The listvenites only occur within a few km of the basal thrust of the ophiolite, and

189 within the tectonic melanges with a serpentine matrix just below the base of the ophiolite (Nasir
190 et al., 2007; Stanger, 1985).

191 *2.2 Lithologies below the Samail ophiolite nappe*

192 Beneath the mantle section of the Samail ophiolite is a locally preserved “metamorphic
193 sole”. This sole is exposed discontinuously along the basal thrust, juxtaposed with the overlying
194 Banded Unit at the base of the Samail mantle section. It records peak metamorphic temperatures
195 of 700-900°C and imprecise peak pressures of 0.8 to 1.4 GPa (Cowan et al., 2014; Hacker &
196 Mosenfelder, 1996; Searle & Cox, 2002; Searle & Malpas, 1980; Soret et al., 2017). A lower
197 temperature unit (~450-550°C) with similar peak pressures (0.8 to 1.2 GPa) has also been
198 identified from the metamorphic section of Oman DP Hole BT1B (Kotowski et al., 2021). The
199 base of the sole is in fault contact with low grade allochthonous sediments of the Hawasina
200 formation, which is composed of pelagic clastic units interlayered with limestones (Bechennec et
201 al., 1988, 1990) deposited from the late Permian to the Cretaceous. The Hawasina sedimentary
202 units were thrust over autochthonous Mesozoic to Proterozoic platform sediments of the
203 Arabian continental margin, forming nappes between the autochthon and the ophiolite.

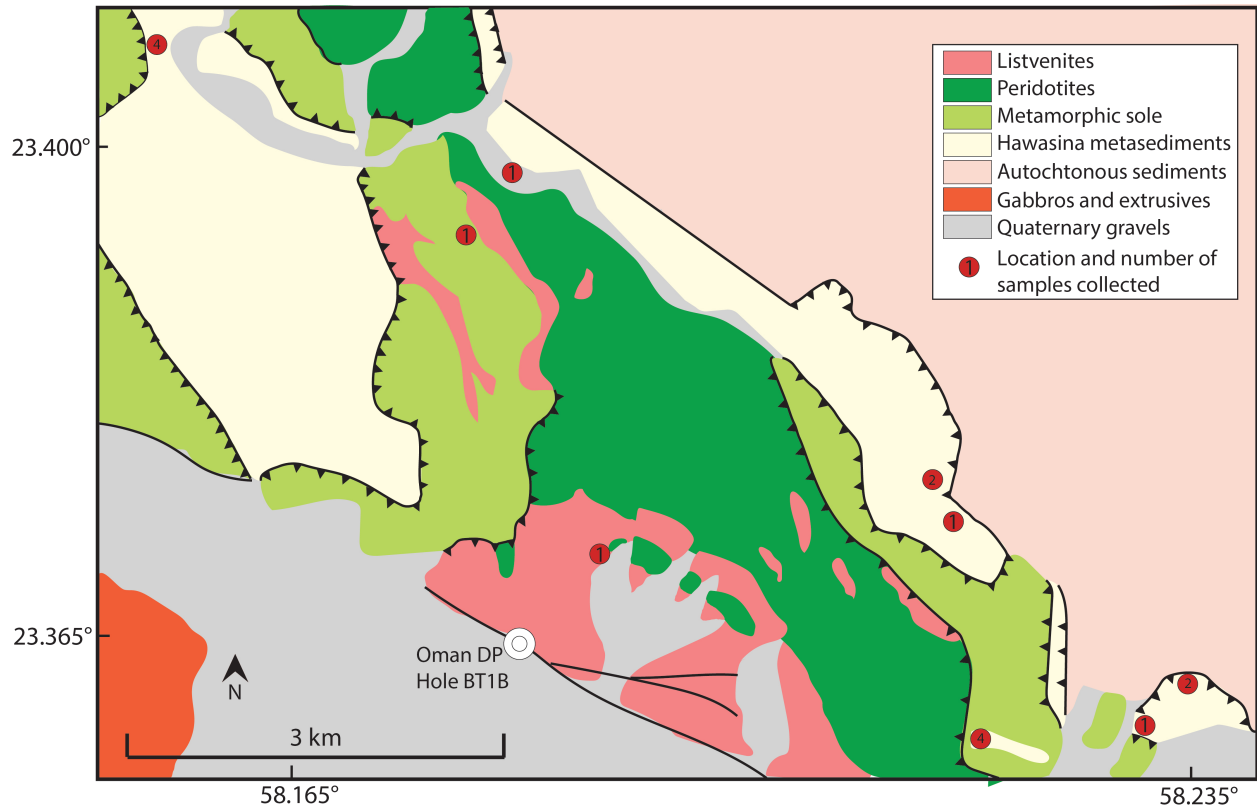
204 *2.3 OmanDP Hole BT1B and Oman Listvenites*

205 Hole BT1B was drilled in March 2017 in Wadi Mansah (23.364374°N, 58.182693°E),
206 which yielded a total length of 300.1 m with 100% recovery (Kelemen et al., 2020). The upper 6
207 meters are composed of alluvial gravels followed by an ultramafic sequence comprised of
208 listvenites (carbonated peridotites) interlayered with two serpentinite bands (80-100 m depth and
209 181 to 186 m depth). A thick (0.42 m) layer of grey-green fault gouge at 196.6 m–197.1 m depth
210 separates the ultramafic units from the metamorphic sole composed of fine-grained metabasalts
211 (Godard et al., 2021; Kelemen et al., 2021; 2020). To the first order, alteration of peridotite to
212 form serpentinite and listvenite in Hole BT1B was nearly isochemical except for the addition of
213 H₂O and CO₂. Average bulk rock Mg/Si, Fe/Si, Al/Si, Fe/Mg, and Cr/Al ratios in serpentinite
214 and listvenite are close to the average composition of the Samail peridotite (Kelemen et al. 2020,
215 2021, Godard et al. 2021) and similar to the composition of previously studied listvenites from
216 the outcrops extending north and northeast from the drill site (Falk & Kelemen, 2015). The core
217 provides a unique record of the interaction between peridotites in the leading edge of the mantle
218 wedge and hydrous fluids rich in CO₂. For an expanded version of the geology of Oman DP Hole
219 BT1B and MoD mountain we refer the reader to the Proceedings of the Oman Drilling Project
220 (Kelemen et al., 2020) and Kelemen et al. (2021).

221 **3 Materials and Methods**

222 Samples analyzed for this study comprise a suite of drill core samples from OmanDP
223 Hole BT1B (listvenites n=50, serpentinites n=14, metamorphic sole rocks n=11) and hand
224 samples of the Hawasina formation (n=18) and metamorphic sole sediments (n=2). Location of
225 Oman DP Hole BT1B and Hawasina samples are shown in Figure 1. Drill core samples
226 encompass all the identified lithologies from Hole BT1B. Major element compositions for Hole
227 BT1B samples were reported in the *Proceedings of the Oman Drilling Project* (Kelemen et al.,
228 2020) with the exception of samples in the 181-186m depth interval which are reported by
229 Godard et al. (2021). Trace element compositions of Hole BT1B samples can be found in

230 Godard et al. (2021). Trace element compositions and loss on ignition for Hawasina formation
 231 outcrop samples were analyzed at Lamont Doherty Earth Observatory (LDEO). Rb and Sr
 232 concentrations were analyzed using a VG PlasmaQuad ExCell quadrupole ICP-MS following
 233 HNO₃-HF digestion. Major element compositions of the Hawasina samples are available in
 234 supplementary table 1. Additional Sr isotopes were measured on samples from outcrops
 235 northeast of Hole BT1B (Falk & Kelemen, 2015).



236
 237 **Figure 1.** Simplified geologic map of Wadi Mansah and vicinity of Oman DP Hole BT1B
 238 compiled after Villey et al. (1986), Google Earth and field observations. Hand samples collected
 239 for this study are marked with red circles with number of samples collected per location in black.

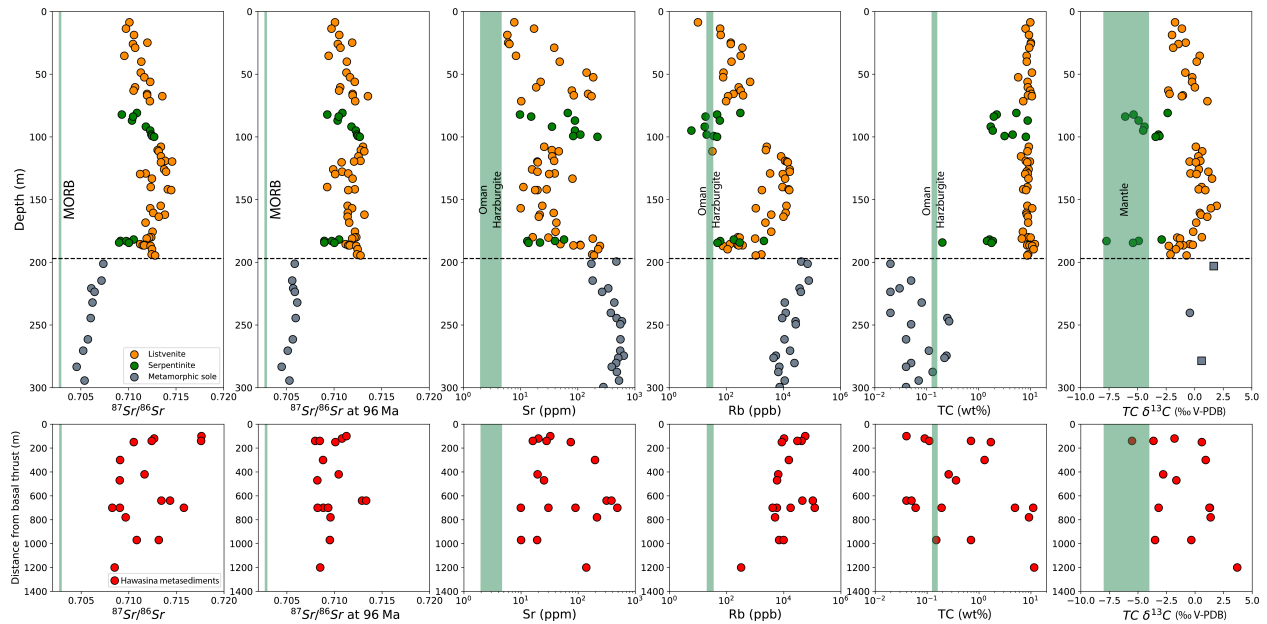
240 For Sr isotope analysis, bulk rock powder was fully digested in a HNO₃-HF mixture
 241 overnight and redissolved in 3N HNO₃ prior to column chemistry using the Eichrom® Sr resin.
 242 Purified Sr were analyzed for isotopic compositions interspersed with US National Institute of
 243 Standards and Technology (NIST) SRM 987 on a Thermo Scientific Neptune multi-collector
 244 ICP-MS at LDEO. In-run mass fractionations were normalized to ⁸⁶Sr/⁸⁸Sr=0.1194. Unknowns
 245 were normalized to SRM 987 ⁸⁷Sr/⁸⁶Sr value of 0.701248. International standards BHVO-2
 246 yielded ⁸⁷Sr/⁸⁶Sr value of 0.703509±41 (2σ, n = 3) and BCR-2 yielded 0.705046±34 (2σ, n = 3),
 247 which agree with published values from Weis et al. (2006).

248 Total Carbon (TC) was measured from the same bulk rock powder splits as for Strontium
 249 isotopes. Total Organic Carbon (TOC, or reduced carbon) was measured from the residual rock
 250 powder after the removal of Inorganic Carbon (carbonate carbon) through reaction with dilute (3
 251 N) HCl for at least 3 days, followed by washing with Millipore® water. Concentrations and δ¹³C

252 ratios of Total Carbon (TC) and Total Organic Carbon (TOC), were determined using a Costech
 253 element analyzer coupled with a Thermo Scientific Delta V plus mass spectrometer at LDEO.
 254 Sample runs were calibrated using Acetanilide for carbon contents ($R^2=0.9998$). For $\delta^{13}\text{C}$ we
 255 used USGS40 ($\delta^{13}\text{C} = -26.77 \pm 0.16\%$ V-PDB, $n=4$), USGS41 ($\delta^{13}\text{C} = 37.63 \pm 0.12\%$ V-PDB, $n=4$)
 256 and USGS24 ($\delta^{13}\text{C} = -16.04 \pm 0.13\%$ V-PDB, $n=4$). All measured values of $\delta^{13}\text{C}$ standards agree
 257 with accepted values reported by the United States Geological Survey (USGS). Inorganic carbon
 258 contents and $\delta^{13}\text{C}$ of total inorganic carbon (TIC) were estimated by mass balance between TC
 259 and TOC.

260 3 Results

261 Depth profiles of $^{87}\text{Sr}/^{86}\text{Sr}$, Sr and Rb concentrations, carbon concentrations, Total
 262 Carbon and Total carbon $\delta^{13}\text{C}$ are shown in Figure 2 and Table 1 and 2. The Hawasina
 263 metasediments are plotted as the horizontal map distance to the closest mapped metamorphic
 264 sole/ultramafic contact.



265

266 **Figure 2.** Depth profiles of OmanDP Hole BT1B (top panels) and distance from basal thrust for
 267 Hawasina metasediments (bottom panels). From left to right $^{87}\text{Sr}/^{86}\text{Sr}$ (measured), $^{87}\text{Sr}/^{86}\text{Sr}$ age
 268 corrected at 96 Ma, Sr concentrations, Rb concentrations, total carbon (TC) concentration, total
 269 carbon $\delta^{13}\text{C}$, (squares in metamorphic sole from Zeko (2021)). Black dashed line in top panels
 270 correspond to basal thrust. Green reference bands in all panels indicate, from left to right:
 271 $^{87}\text{Sr}/^{86}\text{Sr}$ range of MORB (Average $\pm 2\sigma$) (Gale et al., 2013; Hofmann, 2013), Sr and Rb
 272 concentration range of Oman harzburgite (Average $\pm 2\sigma$) (Godard et al., 2000; Hanghøj et al.,
 273 2010; Monnier et al., 2006), total carbon content of Oman harzburgite (Average $\pm 2\sigma$) (Kelemen
 274 & Manning, 2015) and mantle $\delta^{13}\text{C}$ (Average $\pm 2\sigma$) (Deines, 2002). The distance from the basal

275 thrust for the Hawasina metasediments is measured as the horizontal distance to the closest
276 mapped metamorphic sole/ultramafic contact.

277 **Table 1.** Lithological information, depth, strontium, rubidium and carbon concentrations and Sr
278 and C isotope ratios of samples from OmanDP Hole BT1B

279 *Table 1 attached as Excel spreadsheet*

280
281 Abbreviations SE= Standard error, TC= Total Carbon, TOC= Total Organic Carbon, V-PDB= Vienna Pee Dee
282 Belemnite standard, n.d.=not determined

283
284
285 **Table 2.** Lithological information, location, strontium, rubidium and carbon concentrations and
286 Sr and C isotope data of samples for Hawasina and metamorphic sole samples

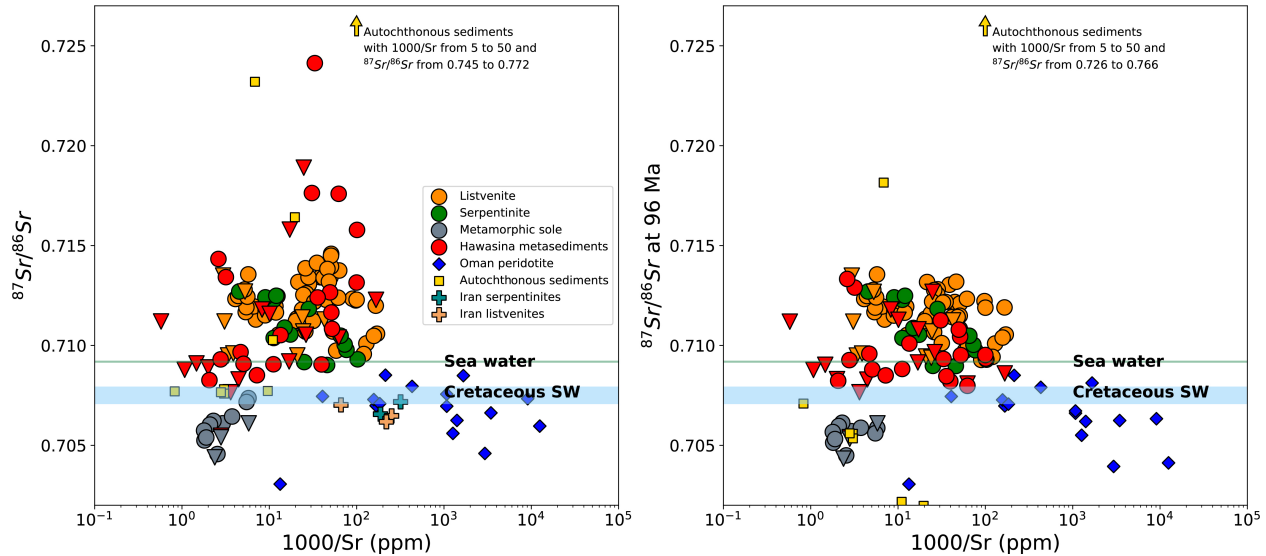
287
288 *Table 2 attached as Excel Spreadsheet*

289
290 Abbreviations SE= Standard error, TC= Total Carbon, T V-PDB= Vienna Pee Dee Belemnite standard,
291 n.a.= not available, n.d.=not determined
292

293 *3.1 Strontium Isotopes*

294 Measured $^{87}\text{Sr}/^{86}\text{Sr}$ values in Oman DP Hole BT1B lithologies show clear differences
295 between (a) the metamorphic sole and (b) the listvenites and serpentinites. The listvenites and
296 serpentinites vary from a minimum value of 0.709 in the upper serpentinite band to a maximum
297 of 0.715 in some listvenites. $^{87}\text{Sr}/^{86}\text{Sr}$ values in the listvenites increase with depth from the
298 surface to 150 m while the serpentinite band between 80-100 m have lower values. Below 150
299 m, $^{87}\text{Sr}/^{86}\text{Sr}$ values are relatively constant with increasing depth, until the second serpentine band
300 at 181-186 m. Below the basal thrust, $^{87}\text{Sr}/^{86}\text{Sr}$ values are significantly lower in the metamorphic
301 sole from 0.704 to 0.706, followed by lower $^{87}\text{Sr}/^{86}\text{Sr}$ values with greater depths (Figure 2).
302 Although the metamorphic sole contains meta-basalts (Godard et al., 2021; Kelemen et al., 2021;
303 Kotowski et al., 2021; Searle & Malpas, 1980), all of the samples have higher $^{87}\text{Sr}/^{86}\text{Sr}$ than
304 typical mid-ocean ridge basalts (MORB) (Gale et al., 2013; Hofmann, 2013). The Sr isotope
305 values of the listvenite and serpentinite samples from BT1B are similar to those of listvenites in
306 nearby outcrops (Falk and Kelemen, 2015, Figure 2), which are significantly more radiogenic
307 than $^{87}\text{Sr}/^{86}\text{Sr}$ values of Oman peridotites (Gerbert-Gaillard, 2002; Lanphere et al., 1981;
308 McCulloch et al., 1981) and Cretaceous to modern seawater (McArthur et al. 2001), but less
309 radiogenic than some Hawasina and autochthonous sediments (Weyhenmeyer, 2000). Our
310 serpentinites and listvenites are enriched in Sr and more radiogenic than similar lithologies in the
311 Birjand ophiolite in eastern Iran (Boskabadi et al., 2020). Our samples of the Hawasina
312 metasediments, and those collected from the same region by Falk and Kelemen (2015) have

313 $^{87}\text{Sr}/^{86}\text{Sr}$ values ranging from 0.7082 to 0.7241. Six of these Hawasina samples are more
 314 radiogenic than any of the samples from Hole BT1B (Figure 3).



315
 316 **Figure 3.** $^{87}\text{Sr}/^{86}\text{Sr}$ values, both measured (left) and age corrected to 96 Ma (right), plotted versus
 317 inverse Sr concentration for core samples from OmanDP Hole BT1B and other lithologies
 318 measured in Oman and Iran. Data from Falk and Kelemen (2015) for samples of the same
 319 lithologies as those documented here are shown as inverted triangles, employing the same color
 320 scheme as used for samples in this study. Data for Hawasina sediments are from this study and
 321 Falk and Kelemen (2015), those for Oman peridotites are from Gerbert-Gaillard (2002, leached
 322 samples only), those for autochthonous sediment samples are from Weyhenmeyer (2000) and
 323 those for Iran samples are from Boskabadi et al. (2020). Rb concentrations were not reported for
 324 the autochthonous clastic metasediments from Weyhenmeyer (2000), so we assume a Rb upper
 325 bound concentration of 200 ppm (twice the maximum measured in Hawasina metasediments).
 326 This Rb concentration was used with the measured $^{87}\text{Sr}/^{86}\text{Sr}$ and Sr concentration, to estimate a
 327 minimum Sr isotope ratio at 96 Ma for these samples. Seawater and Cretaceous seawater values
 328 from McArthur et al. (2001).

329 3.2 Carbon concentrations and $\delta^{13}\text{C}$

330 3.2.1 Total Carbon

331 The carbon contents of samples from Hole BT1B are highly dependent on lithology
 332 (Figure 2). All samples of ultramafic origin contain some carbon, mainly as Mg-rich carbonates,
 333 with serpentinites containing 0.2 to 5 wt% carbon, and listvenites containing 6 to 12 wt%.
 334 Samples from the metamorphic sole below 200 m depth contain 0.02 to 0.27 wt% carbon. In
 335 contrast, the Hawasina metasediments have highly variable carbon contents. Some are almost
 336 pure metamorphosed limestones and dolomites with carbon contents of up to 11 wt%, while
 337 some have less than 0.05 wt% carbon.

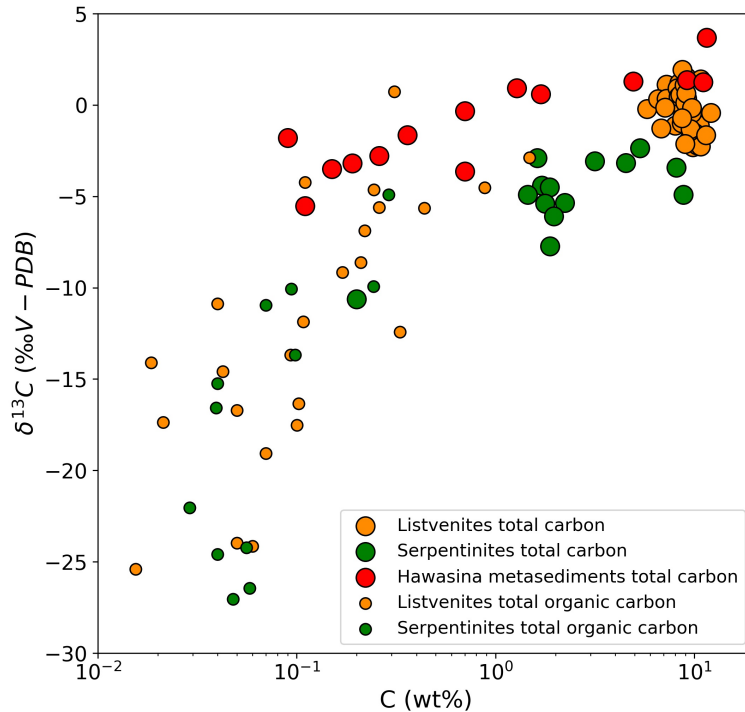
338 $\delta^{13}\text{C}$ in the upper 200m of Hole BT1B varies significantly between serpentinites and
 339 listvenites (Figure 2). Serpentinites contain significantly lighter carbon than listvenites, as

340 observed in the depth profile (Figure 2). The lower serpentinite band contains two samples (74-2
341 0.0-5.0 cm and 74-3 42.0-47.0 cm) that contain significantly lighter carbon than any serpentinite
342 in the upper band. In general, carbon concentrations correlate positively with $\delta^{13}\text{C}$ values in the
343 upper 200 m (Figure 4). Metamorphic sole samples in the bottom 100 m have low carbon
344 contents and did not yield enough CO_2 for isotopic analysis. Total carbon $\delta^{13}\text{C}$ values in the
345 Hawasina nappes range from -5.52‰ to 3.69‰, which almost encompasses the entire range of
346 variation observed in Hole BT1B and appears to decrease with lower carbon contents.

347 *3.2.2 Organic carbon*

348 Graphitic carbon was identified in the core both at the drill site and during core
349 inspection aboard the D/V Chikyu (Kelemen et al, 2020, Kelemen et al. 2021). This organic
350 component has a characteristic low $\delta^{13}\text{C}$ signature in listvenites and serpentinites from Hole
351 BT1B, which extends to a minimum of -27.04‰, representing 0.05wt% of total carbon in the
352 sample from 74-1 56.0-64.0cm (Figure 4). In some cases, the intermediate values likely represent
353 mixtures of organic and inorganic carbon, as some of the magnesite in the listvenites is very
354 resistant to 3N HCl attack and remain undissolved even after 5 days of leaching. The observed
355 light isotopic compositions are similar to those observed in other ultramafic localities such as
356 Cerro de Almirez and Liguria (Alt et al., 2013). These data confirm the presence of organic

357 carbon in Hole BT1B, which was observed during drilling operations, core description aboard
 358 D/V Chikyu and via Raman spectroscopy (Kelemen et al, 2020, Kelemen et al. 2021).



359

360 **Figure 4.** Total Carbon (large circles) and Total Organic Carbon (small circles) versus $\delta^{13}\text{C}$ for
 361 listvenites, serpentinites and Hawasina metasediments.

362 4 Discussion

363 4.1 Temperature and pressure of listvenite formation

364 Falk and Kelemen (2015) estimated the temperature range of listvenite formation based
 365 on conventional and clumped stable isotope thermometry ($90\pm 15^\circ\text{C}$), phase equilibria ($80-$
 366 130°C), and rock textures. New clumped isotope measurements on BT1B drill core samples by
 367 Beinlich et al. (2020) widened the temperature range of listvenite formation and/or cooling from
 368 $\sim 50\pm 5^\circ\text{C}$ to $250\pm 50^\circ\text{C}$. This range of values suggests that the infiltrating reactive fluids had
 369 variable temperatures, and/or clumped isotope values were reset during cooling, as proposed for
 370 fine-grained samples of peridotite-hosted carbonate veins (Garcia del Real et al., 2016). The
 371 pressure of listvenite formation is very poorly constrained due to the lack of pressure-sensitive
 372 assemblages and the small size of fluid inclusions. A minimum pressure of 0.3 GPa is provided
 373 by the P-T conditions recorded by the Arabian carbonate platform during ophiolite obduction
 374 (Grobe et al., 2019). For the upper limit, the listvenites must have formed at a pressure below the

375 maximum pressure reported for the metamorphic sole (~ 1.4 GPa) (Cowan et al., 2014; Searle
376 and Cox, 2002).

377 *4.2 Timing of listvenite formation*

378 Falk and Kelemen (2015) used Rb/Sr and $^{87}\text{Sr}/^{86}\text{Sr}$ data on mineral separates to produce
379 an imprecise isochron age of 97 ± 29 Ma for a listvenite sample. This age is broadly consistent
380 with the ~96 Ma age of formation of igneous crust in the ophiolite, along with the same age of
381 metamorphism for the underlying metamorphic sole just beneath the basal thrust of the ophiolite
382 (Hacker, 1994; Hacker et al., 1996; Rioux et al., 2013, 2016). Moreover, listvenites are found in
383 and near the basal thrust, from the UAE near the northwestern end of the ophiolite outcrop to the
384 area around Hole BT1B, near the southeastern end of the ophiolite outcrop in Oman (Nasir et al.,
385 2007; Stanger, 1985). The extensive outcrop NE of Hole BT1B, known informally as MoD
386 Mountain, exposes the Banded Horizon, a peridotite unit found at the base of the ophiolite
387 mantle section composed of alternating 1- to 10-meter scale bands of dunite, harzburgite, and
388 minor lherzolite. This unit has distinct geochemical characteristics, with higher Al and middle
389 rare-earth-elements, compared to the residual mantle harzburgites that comprise most of the
390 mantle section of the ophiolite (Boudier et al., 1988; Godard et al., 2021; Khedr et al., 2014;
391 Prigent et al., 2018; Yoshikawa et al., 2015). The BT1B listvenites have compositions suggesting
392 that they were formed after basal peridotites from the Banded Horizon (Godard et al., 2021).

393 Throughout this region, the contacts of listvenite bands within and at the base of the
394 Banded Unit are broadly parallel to banding in the peridotite, and to the contacts between
395 listvenite, peridotite, metamorphic sole, and the Hawasina nappe. These data are consistent with
396 our hypothesis that most of the listvenites formed by alteration of mantle peridotite during the
397 subduction of the underlying sediments via intra-oceanic thrusting and/or later emplacement of
398 the ophiolite onto the Arabian continental margin.

399 On the basis of steep, fault-bounded contacts of listvenite with young, post-emplacement
400 conglomerates, several workers have inferred that the listvenites formed during later uplift and
401 extension (Nasir et al., 2007; Stanger, 1985; Wilde et al., 2002). Recently, Scharf et al. (2020)
402 reported 60 ± 16 Ma and 58 ± 6 Ma U/Pb ages for two carbonate veins that cut listvenite, and
403 structural observations indicating a top-down sense of shear along some faulted listvenite-
404 peridotite and listvenite-sole contacts. Following prior interpretations, they interpret these ages
405 as formation ages of the listvenites after ophiolite emplacement during uplift of the nearby Jebel
406 Akdar and Saih Hatat anticlinoria. We find that their interpretation is inconsistent with the field
407 observations reported above and evidence of a multistage tectonic overprint after peridotite
408 carbonation and listvenite formation as reported by Menzel et al. (2020) and Kelemen et al.
409 (2020).

410 We have age-corrected our $^{87}\text{Sr}/^{86}\text{Sr}$ to the 96 Ma age reported by Falk and Kelemen
411 (2015). This correction gives the lowest possible $^{87}\text{Sr}/^{86}\text{Sr}$ for all the samples based on reported
412 ages. For the corrections, we used Sr and Rb concentrations reported by Godard et al. (2021) for
413 Hole BT1B and our analyses of Hawasina metasediments. While Rb/Sr is low in most BT1B
414 samples and thus age corrections are small, this correction removes some of the apparent trends
415 observed in measured $^{87}\text{Sr}/^{86}\text{Sr}$ versus depth. The age corrections particularly affect listvenites
416 with relatively abundant chromian mica (fuchsite-muscovite solid solutions, Falk & Kelemen

417 2015, supplement) in the 115-163 m depth interval, as these micas host abundant Rb (Godard et
418 al. 2021). The age correction also affects the estimated $^{87}\text{Sr}/^{86}\text{Sr}$ values of the metamorphic sole
419 of BT1B and some of the Hawasina metasediments as their Sr and Rb concentrations are
420 heterogeneous, ranging from 9 to 638 ppm for Sr and 0.4 to 97.7 ppm for Rb. Regardless, the
421 age-corrected $^{87}\text{Sr}/^{86}\text{Sr}$ values of the listvenites are much higher than those of the mantle and
422 Cretaceous seawater.

423 *4.3 Fluid source for carbonation of peridotites in Oman DP Hole BT1B*

424 $^{87}\text{Sr}/^{86}\text{Sr}$ and d^{13}C data on MoD Mountain listvenites and Hole BT1B samples suggest
425 that replacement of peridotite by serpentinite and listvenite resulted from reaction with a single
426 fluid along a reaction path (Kelemen et al., 2021). The initial fluid was far from equilibrium with
427 peridotite, which converted olivine and serpentine in the protolith to carbonates + quartz and
428 approached equilibrium with serpentinite at higher extents of reaction progress and lower
429 integrated water/rock ratios (Beinlich et al., 2020, Kelemen et al., 2021). Mg isotope data from a
430 set of samples studied by Falk and Kelemen (2015) show significant differences between
431 dolomite and magnesite listvenites. Dolomite listvenites (average $\delta^{26}\text{Mg} \sim -1.33\text{‰}$) are lighter in
432 Mg isotopes than magnesite listvenites (average $\delta^{26}\text{Mg} \sim -0.33\text{‰}$) (de Obeso et al., 2021), which
433 suggests magnesite dissolution and dolomite formation. This is consistent with the modelled
434 evolution of listvenites during fluid-rock reaction, with dolomite replacing magnesite at
435 increasing water/rock ratios (Kelemen et al., 2021). The process of formation of dolomite veins
436 at the expense of magnesite has been documented in other Cretaceous ophiolites (Boskabadi et
437 al., 2020).

438 As noted above, after the magnesite and dolomite listvenites formed they were
439 cataclastically deformed, and then cut by late Ca-rich carbonate veins (Menzel et al. 2020). Thus,
440 one might expect the veins to have formed from a later, geochemically distinctive fluid as
441 suggested by variable clumped isotope ($\Delta 47$) derived temperatures (Beinlich et al., 2020) and
442 changes in geochemical signatures in dolomite-dominated intervals (Godard et al. 2021). This
443 can be further addressed in future studies via careful sampling of the post-cataclastic veins and
444 dolomite-rich domains.

445 Returning attention to the source of the fluid that formed the bulk of the listvenites,
446 assuming that Sr and CO_2 were derived from the same fluid, Sr isotopes can be used to constrain
447 the source of the carbonating fluids that formed the serpentinites and listvenites. Falk and
448 Kelemen (2015) proposed three possible sources of fluids for carbonation: (1) compaction of
449 pore waters from underlying Hawasina metasediments, (2) low temperature dehydration of opal
450 and clay minerals in calcite-bearing Hawasina metasediments, and (3) higher-grade metamorphic
451 devolatilization reactions involving subducted sediments similar to the Hawasina metasediments
452 coupled with fluid that migrated up the subduction zone.

453 Unlike younger, mantle-peridotite-hosted carbonates, the listvenites do not contain a
454 significant fraction of seawater- or groundwater-derived Sr (Gerbert-Gaillard, 2002; Kelemen et
455 al., 2011; de Obeso & Kelemen, 2018; Weyhenmeyer, 2000). The listvenites have $^{87}\text{Sr}/^{86}\text{Sr}$ ratios
456 that are distinct from recent, low-temperature carbonate veins and travertine in the mantle section
457 of the ophiolite (Kelemen et al., 2011; de Obeso & Kelemen, 2018; Weyhenmeyer, 2000).
458 Almost all of the listvenites and associated serpentinites from BT1B core and MoD Mountain

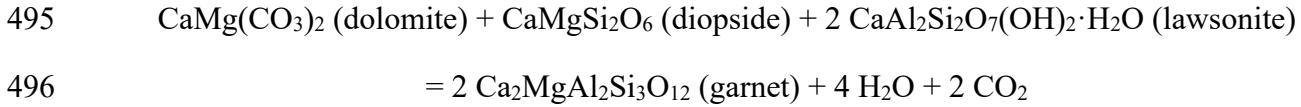
459 outcrops have $^{87}\text{Sr}/^{86}\text{Sr}$ ratios at 96 Ma higher than Cretaceous seawater (Falk & Kelemen 2015,
460 and this paper). In contrast, young, peridotite-hosted carbonate veins and travertines in the
461 Samail ophiolite consistently have $^{87}\text{Sr}/^{86}\text{Sr}$ lower than 0.709 and appear to contain mixtures of
462 Sr derived from seawater or groundwater and the mantle (Gerbert-Gaillard, 2002; Kelemen et al.,
463 2011; de Obeso & Kelemen, 2018; Weyhenmeyer, 2000).

464 Core samples of the sole have $^{87}\text{Sr}/^{86}\text{Sr}$ ratios that are similar to Indian Ocean MORB and
465 near-ridge Pacific seamounts (Hofmann, 2013), which are systematically lower than the Sr
466 isotope ratios of the listvenites. Perhaps the metamorphic sole metabasalts are remnants of a
467 subducted seamount, similar to accreted seamounts along the Cascadia margin of North America
468 (e.g., Duncan, 1982), which derived from the enriched mantle source of some Indian Ocean
469 MORB. Alternatively, the $^{87}\text{Sr}/^{86}\text{Sr}$ ratios may have increased during alteration. The stark
470 difference in $^{87}\text{Sr}/^{86}\text{Sr}$ between the metamorphic sole and the listvenites indicates that fluids
471 derived from the sole are not responsible of the $^{87}\text{Sr}/^{86}\text{Sr}$ enrichment observed in the ultramafic
472 lithologies in Wadi Mansah.

473 In contrast, age-corrected Sr isotope ratios for Hawasina metasediments underlying the
474 ophiolite and the metamorphic sole, north and northeast of Hole BT1B, have $^{87}\text{Sr}/^{86}\text{Sr}$ up to
475 0.7134 at 96 Ma (Figure 2). The samples with the most radiogenic $^{87}\text{Sr}/^{86}\text{Sr}$ are clastic sediments
476 containing minor amounts of carbonates. Hawasina limestones, on the other hand, have lower
477 $^{87}\text{Sr}/^{86}\text{Sr}$ values, which is consistent with calcite precipitated from seawater that incorporated a
478 minor, radiogenic clastic component. Based on these observations, the most likely source of the
479 fluids that formed the listvenites are derived from the Hawasina metasediments.

480 Thermodynamic modeling of fluid-rock reactions (Kelemen et al. 2021) shows that the
481 characteristic listvenite mineral assemblages – magnesite + quartz – are attained from fluids with
482 ~20,000 ppm dissolved C for listvenite formation at 100-300 °C and 0.5 to 1 GPa, similar to the
483 assemblages modeled by Klein and Garrido (2011) at lower pressures. Such high dissolved
484 carbon contents are impossible to attain by congruent dissolution of pure calcite in aqueous
485 fluids at these P-T conditions (Kelemen & Manning, 2015), which rules out silicate-poor
486 limestones such as those from the continental margin as a carbon source. On the other hand,
487 metamorphic devolatilization of rocks composed of silicate-carbonate mixtures can produce C-
488 rich fluids at temperatures above 400 °C and low to moderate pressures, depending on the rock
489 composition. Thus, we infer that the fluids that formed the listvenites derived from
490 devolatilization of subducting metasediments. During prograde subduction metamorphism, calc-
491 silicate rocks, containing both clastic and carbonate components, undergo extensive
492 devolatilization at 2-3 GPa and 500 to 700°C (Gorman et al., 2006; Stewart & Ague, 2020) and

493 lose significant amounts of their CO₂ in this PT range due to reactions similar to the simplified
494 reaction:



497 In contrast, carbonate-rich compositions (limestone, dolomite, marble) are predicted to
498 retain most of their CO₂ during subduction (e.g, Kerrick & Connolly, 2001; Stewart & Ague,
499 2020).

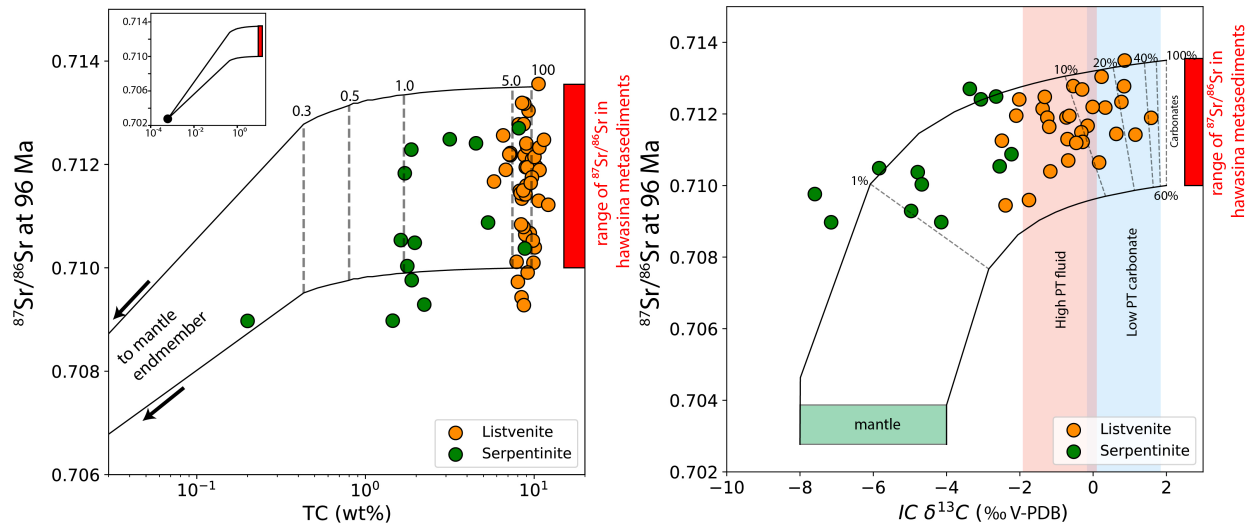
500 These decarbonation reactions are possible for both the metamorphic sole and Hawasina
501 sediments. The modelling approach of Kelemen et al. (2021) suggests that fluids derived from
502 the sole and clastic Hawasina metasediments will have enough dissolved carbon to react with
503 peridotite and result in magnesite-quartz rocks, the characteristic listvenite assemblage.
504 However, if fluids derived from the sole are the source of the carbon, admixing of a different
505 fluid derived from Hawasina metasediments is required to explain the ⁸⁷Sr/⁸⁶Sr measured in the
506 listvenites. On the other hand, Kelemen et al. show that fluids derived from a rock with
507 composition analogous to Hawasina OM20-17 contain enough dissolved carbon for
508 serpentinization and carbonation of peridotite with increasing water/rock (W/R) ratios. This,
509 combined with the radiogenic ⁸⁷Sr/⁸⁶Sr composition of OM20-17, suggests that a single fluid
510 could be responsible for carbonation of the peridotites. We test this scenario using the reaction
511 path proposed by Kelemen et al. (2021). Their model generates a fluid with ~14,000 ppm carbon
512 at 400°C and 1GPa from decarbonation of a rock with composition such as OM20-17. Under
513 these modelled conditions (400 °C, 1 GPa) a lithology like OM20-17 will lose ~65% of its
514 carbon, other Hawasina samples require less decarbonation to produce fluids capable of
515 carbonating the peridotites. If this fluid is then cooled to 200°C and depressurized to 0.5GPa
516 without losing much of its carbon before reacting with peridotites, listvenites are predicted to
517 form at water/rock (W/R)~100.

518 At temperatures greater than ~ 300°C, dissolved CO₂ in aqueous fluids have δ¹³C values
519 that are higher than those of co-existing calcite and dolomite (Chacko et al., 1991; Deines, 2004;
520 Horita, 2014). Thus, for example, fluid in equilibrium with calcite with δ¹³C between -5.5‰ to -
521 3.5‰ (as in Hawasina clastic metasediments) would contain dissolved CO₂ with δ¹³C of -1.9‰
522 to 0.1‰ at 400°C. At lower temperatures, like those estimated for listvenite formation in the
523 Samail ophiolite, calcite and dolomite have δ¹³C higher than co-existing fluids. Thus, dolomite
524 and magnesite in equilibrium with fluids with δ¹³C of -1.9‰ to 0.1‰ would have δ¹³C in the
525 range of -0.2‰ to 1.8‰, similar to the δ¹³C observed in the listvenites from Hole BT1B and the
526 surrounding outcrops.

527 Figure 5a illustrates that the listvenites and serpentinites from Hole BT1B lie along the
528 reaction path used by Kelemen et al., (2021). In our calculations, we assume that reacting fluids
529 enriched in Sr (250 ppm), with ⁸⁷Sr/⁸⁶Sr values at 96 Ma that are similar to those of clastic
530 Hawasina metasediments (0.7110 to 0.7135), reacted with the peridotite with mantle-like
531 ⁸⁷Sr/⁸⁶Sr (0.7027±0.0011). In the model serpentinites plot at low W/R between 1 to 5 while
532 listvenites require significantly more fluid at W/R between 5-100. The listvenites and
533 serpentinites follow a mixing trend (Figure 5b) between mantle peridotite like compositions

534 (Sr=1.5 ppm, $^{87}\text{Sr}/^{86}\text{Sr}=0.7027\pm 0.0011$, C=680ppm and $\delta^{13}\text{C}=-6.0\pm 2.0\%$) and low temperature
 535 carbonates that crystallized from a fluid produced by high-pressure, high-temperature
 536 devolatilization with Sr isotope ratios in the range of the Hawasina clastic metasediments
 537 (Sr=250ppm, $^{87}\text{Sr}/^{86}\text{Sr}\sim 0.7100$ to 0.7135) and fractionate carbon isotopes as described above.
 538 These trends together suggest that the CO_2 -bearing aqueous fluids that formed the listvenites
 539 from Hole BT1B and surrounding outcrops were derived by devolatilization of calc-silicate
 540 metasediments, with $^{87}\text{Sr}/^{86}\text{Sr}$ and $\delta^{13}\text{C}$ similar to clastic sediments in the Hawasina Formation
 541 along a subduction zone geotherm. These fluids migrated updip to lower pressures and
 542 temperatures to form the listvenites.

543



544

545 **Figure 5.** (left) Total carbon (wt%) vs. $^{87}\text{Sr}/^{86}\text{Sr}$ at 96 Ma. Black lines are reaction paths of
 546 carbon rich fluid reacting with peridotite at 200°C and 0.5GPa at variable water/rock (dashed tie
 547 lines) from Kelemen et al. (2021). The reacting fluid is assumed to have $^{87}\text{Sr}/^{86}\text{Sr}$ values of
 548 0.7100 to 0.7135 like those of clastic Hawasina metasediments. (right) Inorganic carbon $\delta^{13}\text{C}$ vs.
 549 $^{87}\text{Sr}/^{86}\text{Sr}$ at 96 Ma. Black lines are mixing lines between mantle and carbonate minerals
 550 precipitated from a metamorphic fluid. The fluid has the same carbon concentration as the
 551 reaction path on the figure 5a and the $\delta^{13}\text{C}$ fractionation between the carbonate and the fluid are
 552 described in the body of the text, with values for high and low PT shown as red and blue boxes
 553 respectively. We assume that the fluid has the Sr isotope ratios of Hawasina clastic
 554 metasediments. $^{87}\text{Sr}/^{86}\text{Sr}$ values for the depleted mantle are from mid-ocean-ridge-basalt
 555 (MORB) from Hofmann (2013). Mantle $\delta^{13}\text{C}$ is from Deines (2002).

556 5 Conclusions

557 Listvenites and spatially associated serpentinites from Hole BT1B and surrounding
 558 outcrops that replace residual mantle peridotites from the base of the Samail ophiolite have Sr
 559 isotope ratios that are more radiogenic than their peridotite protoliths, Cretaceous seawater,
 560 modern seawater, groundwater in the ophiolite, and the underlying metamorphic sole. We
 561 suggest that the radiogenic Sr isotope component was transported via carbon-rich aqueous fluid
 562 that reacted with the peridotite to form the listvenites and serpentinites. The $^{87}\text{Sr}/^{86}\text{Sr}$ values of

563 this component resemble those of calcite-bearing clastic sediments in the Hawasina Formation
564 underlying the ophiolite. However, the fluid must have contained higher dissolved carbon
565 contents than feasible for congruent dissolution of pure calcite at < 2 GPa and/or < 550°C. Thus,
566 we hypothesize that this fluid was derived by devolatilization of carbonate- and silicate bearing
567 meta-sediments akin to the Hawasina clastic metasediments at 0.5 to 2.3 GPa and 400 to 700°C
568 in the subduction zone (Searle et al., 1994). This fluid then migrated updip to react with hanging
569 wall peridotite at <1 GPa and <250°C, forming the listvenites and serpentinites. Carbon isotope
570 fractionation during high temperature devolatilization followed by low temperature carbonate
571 precipitation during the reaction with peridotite likely controlled the isotopic characteristics of
572 the listvenites and the serpentinites with $\delta^{13}\text{C}$ from -10.6‰ to 1.92‰ and $^{87}\text{Sr}/^{86}\text{Sr}$ from 0.7090
573 to 0.7145.

574 **6 Acknowledgments and Data**

575 JCO wants to thank Steven Goldstein for allowing early access to the laboratories in LDEO to
576 complete isotope work soon after partial reopening following the first wave of the COVID-19
577 pandemic in New York. JCO work to complete this manuscript at UCalgary was in part funded
578 from the Canada First Research Excellence Fund. Wei Huang is thanked for help with
579 measurements of carbon concentrations and $\delta^{13}\text{C}$. We thank Mark Dekkers for editorial handling.
580 Constructive comments from an anonymous Associate Editor, Arman Boskabadi and an
581 anonymous reviewer helped to improve an earlier versions of this manuscript. This research used
582 samples and/or data provided by the Oman Drilling Project. The Oman Drilling Project (OmanDP)
583 has been possible through co-mingled funds from the International Continental Scientific Drilling
584 Project (ICDP; Kelemen, Matter, Teagle Lead PIs), the Sloan Foundation – Deep Carbon
585 Observatory (Grant 2014-3-01, Kelemen PI), the National Science Foundation (NSF-EAR-
586 1516300, Kelemen lead PI), NASA – Astrobiology Institute (NNA15BB02A, Templeton PI), the
587 German Research Foundation (DFG: KO 1723/21-1, Koepke PI), the Japanese Society for the
588 Promotion of Science (JSPS no:16H06347, Michibayashi PI; and KAKENHI 16H02742,
589 Takazawa PI), the European Research Council (Adv: no.669972; Jamveit PI), the Swiss National
590 Science Foundation (SNF:20FI21_163073, Früh-Green PI), JAMSTEC, the TAMU-JR Science
591 Operator, and contributions from the Sultanate of Oman Ministry of Regional Municipalities and
592 Water Resources, the Oman Public Authority of Mining, Sultan Qaboos University, CNRS-Univ.
593 Montpellier, Columbia University of New York, and the University of Southampton.

594 Authors declare no conflict of interest.

595 All data is in the process of being approved by Pangea repository:
596 <https://issues.pangaea.de/browse/PDI-30281> and <https://issues.pangaea.de/browse/PDI-30282>

597

598 **7 References**

599 Alt, J. C., Schwarzenbach, E. M., Früh-Green, G. L., Shanks, W. C., Bernasconi, S. M., Garrido,
600 C. J., et al. (2013). The role of serpentinites in cycling of carbon and sulfur: Seafloor
601 serpentinitization and subduction metamorphism. *Lithos*, 178, 40–54.
602 <https://doi.org/10.1016/j.lithos.2012.12.006>

- 603 Bach, W., Rosner, M., Jöns, N., Rausch, S., Robinson, L. F., Paulick, H., & Erzinger, J. (2011).
 604 Carbonate veins trace seawater circulation during exhumation and uplift of mantle rock:
 605 Results from ODP Leg 209. *Earth and Planetary Science Letters*, 311(3–4), 242–252.
 606 <https://doi.org/10.1016/j.epsl.2011.09.021>
- 607 Bechennec, F., Le Métour, J., Rabu, D., Villey, M., & Beurrier, M. (1988). The Hawasina Basin:
 608 A fragment of a starved passive continental margin, thrust over the Arabian Platform during
 609 obduction of the Sumail Nappe. *Tectonophysics*, 151(1–4). [https://doi.org/10.1016/0040-1951\(88\)90251-X](https://doi.org/10.1016/0040-1951(88)90251-X)
- 611 Bechennec, F., Le Metour, J., Rabu, D., Bourdillon-de-Grissac, C., de Wever, P., Beurrier, M., &
 612 Villey, M. (1990). The Hawasina Nappes: Stratigraphy, palaeogeography and structural
 613 evolution of a fragment of the south-Tethyan passive continental margin. *Geological*
 614 *Society Special Publication*, 49(49), 213–223.
 615 <https://doi.org/10.1144/GSL.SP.1992.049.01.14>
- 616 Beinlich, A., Plümper, O., Havelmann, J., Austrheim, H., & Jamtveit, B. (2012). Massive
 617 serpentinite carbonation at Linnajavri, N-Norway. *Terra Nova*, 24(6), 446–455.
 618 <https://doi.org/10.1111/j.1365-3121.2012.01083.x>
- 619 Beinlich, A., Plümper, O., Boter, E., Müller, I. A., Kourim, F., Ziegler, M., et al. (2020).
 620 Ultramafic Rock Carbonation: Constraints From Listvenite Core BT1B, Oman Drilling
 621 Project. *Journal of Geophysical Research: Solid Earth*, 125(6), 1–21.
 622 <https://doi.org/10.1029/2019jb019060>
- 623 Blakely, R. J., Brocher, T. M., & Wells, R. E. (2005). Subduction-zone magnetic anomalies and
 624 implications for hydrated forearc mantle. *Geology*, 33(6), 445–448.
 625 <https://doi.org/10.1130/G21447.1>
- 626 Boskabadi, A., Pitcairn, I. K., Broman, C., Boyce, A., Teagle, D. A. H., Cooper, M. J., et al.
 627 (2017). Carbonate alteration of ophiolitic rocks in the Arabian–Nubian Shield of Egypt:
 628 sources and compositions of the carbonating fluid and implications for the formation of Au
 629 deposits. *International Geology Review*, 59(4), 391–419.
 630 <https://doi.org/10.1080/00206814.2016.1227281>
- 631 Boskabadi, A., Pitcairn, I. K., Leybourne, M. I., Teagle, D. A. H., Cooper, M. J., Hadizadeh, H.,
 632 et al. (2020). Carbonation of ophiolitic ultramafic rocks: Listvenite formation in the Late
 633 Cretaceous ophiolites of eastern Iran. *Lithos*, 352–353, 105307.
 634 <https://doi.org/10.1016/j.lithos.2019.105307>
- 635 Boudier, F., Ceuleneer, G., & Nicolas, A. (1988). Shear zones, thrusts and related magmatism in
 636 the Oman ophiolite: Initiation of thrusting on an oceanic ridge. *Tectonophysics*, 151(1–4),
 637 275–296. [https://doi.org/10.1016/0040-1951\(88\)90249-1](https://doi.org/10.1016/0040-1951(88)90249-1)
- 638 Braun, M. G. (2004). *Petrologic and Microstructural Constraints on Focused Melt Transport in*
 639 *Dunites and Rheology of the Shallow Mantle*. WHOI/MIT. Retrieved from
 640 <http://oai.dtic.mil/oai/oai?verb=getRecord&metadataPrefix=html&identifier=ADA426948>
- 641 Braun, M. G., & Kelemen, P. B. (2002). Dunite distribution in the Oman Ophiolite: Implications
 642 for melt flux through porous dunite conduits. *Geochemistry, Geophysics, Geosystems*,
 643 3(11), 1–21. <https://doi.org/10.1029/2001GC000289>
- 644 Chacko, T., Mayeda, T. K., Clayton, R. N., & Goldsmith, J. R. (1991). Oxygen and carbon

- 645 isotope fractionations between CO₂ and calcite. *Geochimica et Cosmochimica Acta*, 55(10),
646 2867–2882. [https://doi.org/10.1016/0016-7037\(91\)90452-B](https://doi.org/10.1016/0016-7037(91)90452-B)
- 647 Clark, I. D., & Fontes, J.-C. (1990). Paleoclimatic reconstruction in northern Oman based on
648 carbonates from hyperalkaline groundwaters. *Quaternary Research*, 33(3), 320–336.
649 [https://doi.org/10.1016/0033-5894\(90\)90059-T](https://doi.org/10.1016/0033-5894(90)90059-T)
- 650 Collier, M. L. (2012). *Spatial-Statistical Properties of Geochemical Variability as Constraints*
651 *on Magma Transport and Evolution Processes at Ocean Ridges*. Columbia University.
- 652 Cowan, R. J., Searle, M. P., & Waters, D. J. (2014). Structure of the metamorphic sole to the
653 Oman Ophiolite, Sumeini Window and Wadi Tayyin: Implications for ophiolite obduction
654 processes. *Geological Society Special Publication*, 392(1), 155–175.
655 <https://doi.org/10.1144/SP392.8>
- 656 Deines, P. (2002). The carbon isotope geochemistry of mantle xenoliths. *Earth-Science Reviews*,
657 58(3–4), 247–278. [https://doi.org/10.1016/S0012-8252\(02\)00064-8](https://doi.org/10.1016/S0012-8252(02)00064-8)
- 658 Deines, P. (2004). Carbon isotope effects in carbonate systems. *Geochimica et Cosmochimica*
659 *Acta*, 68(12), 2659–2679. <https://doi.org/10.1016/j.gca.2003.12.002>
- 660 Delacour, A., Früh-Green, G. L., Bernasconi, S. M., Schaeffer, P., & Kelley, D. S. (2008).
661 Carbon geochemistry of serpentinites in the Lost City Hydrothermal System (30°N, MAR).
662 *Geochimica et Cosmochimica Acta*, 72(15), 3681–3702.
663 <https://doi.org/10.1016/J.GCA.2008.04.039>
- 664 DeShon, H. R., & Schwartz, S. Y. (2004). Evidence for serpentinization of the forearc mantle
665 wedge along the Nicoya Peninsula, Costa Rica. *Geophysical Research Letters*, 31(21), 2–5.
666 <https://doi.org/10.1029/2004GL021179>
- 667 Falk, E. S., & Kelemen, P. B. (2015). Geochemistry and petrology of listvenite in the Samail
668 ophiolite, Sultanate of Oman: Complete carbonation of peridotite during ophiolite
669 emplacement. *Geochimica et Cosmochimica Acta*, 160, 70–90.
670 <https://doi.org/10.1016/j.gca.2015.03.014>
- 671 Früh-Green, G. L., Connolly, J. A. D. D., Plas, A., Kelley, D. S., Grobety, B., Früh-Green, G. L.,
672 et al. (2004). Serpentinization of oceanic peridotites: Implications for geochemical cycles
673 and biological activity. In *AGU Monograph* (Vol. 144, pp. 119–136).
674 <https://doi.org/10.1029/144GM08>
- 675 Gale, A., Dalton, C. A., Langmuir, C. H., Su, Y., & Schilling, J. G. (2013). The mean
676 composition of ocean ridge basalts. *Geochemistry, Geophysics, Geosystems*, 14(3), 489–
677 518. <https://doi.org/10.1029/2012GC004334>
- 678 Garcia del Real, P., Maher, K., Kluge, T., Bird, D. K., Brown, G. E., & John, C. M. (2016).
679 Clumped-isotope thermometry of magnesium carbonates in ultramafic rocks. *Geochimica et*
680 *Cosmochimica Acta*, 193, 222–250. <https://doi.org/10.1016/j.gca.2016.08.003>
- 681 Gerbert-Gaillard, L. (2002). *Caractérisation Géochimique des Péridotites de l'ophiolite*
682 *d'Oman : processus magmatiques aux limites lithosphère/asthenosphère*. Université
683 Montpellier II - Sciences et Techniques du Languedoc.
- 684 Godard, M., Joussetin, D., & Bodinier, J.-L. (2000). Relationships between geochemistry and
685 structure beneath a palaeo-spreading centre: a study of the mantle section in the Oman

- 686 ophiolite. *Earth and Planetary Science Letters*, 180(1–2), 133–148.
 687 [https://doi.org/10.1016/S0012-821X\(00\)00149-7](https://doi.org/10.1016/S0012-821X(00)00149-7)
- 688 Godard, M., Carter, E., Decrausaz, T., Lafay, R., Bennett, E., Kourim, F., et al. (2021).
 689 Geochemical Profiles Across the Listvenite-Metamorphic Transition in the Basal
 690 Megathrust of the Semail Ophiolite: Results from Drilling at Oman DP Hole BT1B. *Earth
 691 and Space Science Open Archive*. <https://doi.org/https://doi.org/10.1002/essoar.10507497.1>
- 692 Gorman, P. J., Kerrick, D. M., & Connolly, J. a. D. (2006). Modeling open system metamorphic
 693 decarbonation of subducting slabs. *Geochemistry, Geophysics, Geosystems*, 7(4).
 694 <https://doi.org/10.1029/2005GC001125>
- 695 Grobe, A., Von Hagke, C., Littke, R., Dunkl, I., Wübbeler, F., Muchez, P., & Urai, J. L. (2019).
 696 Tectono-Thermal evolution of Oman’s Mesozoic passive continental margin under the
 697 obducting Semail Ophiolite: A case study of Jebel Akhdar, Oman. *Solid Earth*, 10(1), 149–
 698 175. <https://doi.org/10.5194/se-10-149-2019>
- 699 Hacker, B. R. (1994). Rapid Emplacement of Young Oceanic Lithosphere: Argon
 700 Geochronology of the Oman Ophiolite. *Science*, 265(5178), 1563–1565.
 701 <https://doi.org/10.1126/science.265.5178.1563>
- 702 Hacker, B. R., & Mosenfelder, J. L. (1996). Metamorphism and deformation along the
 703 emplacement thrust of the Samail ophiolite, Oman. *Earth and Planetary Science Letters*,
 704 144(3–4), 435–451. [https://doi.org/10.1016/S0012-821X\(96\)00186-0](https://doi.org/10.1016/S0012-821X(96)00186-0)
- 705 Hacker, B. R., Mosenfelder, J. L., & Gnos, E. (1996). Rapid emplacement of the Oman ophiolite:
 706 Thermal and geochronologic constraints. *Tectonics*, 15(6), 1230–1247.
 707 <https://doi.org/10.1029/96TC01973>
- 708 Halls, C., & Zhao, R. (1995). Listvenite and related rocks: perspectives on terminology and
 709 mineralogy with reference to an occurrence at Cregganbaun, Co. Mayo, Republic of Ireland.
 710 *Mineralium Deposita*, 30(3–4), 303–313. <https://doi.org/10.1007/BF00196366>
- 711 Hanghøj, K., Kelemen, P. B., Hassler, D., & Godard, M. (2010). Composition and Genesis of
 712 Depleted Mantle Peridotites from the Wadi Tayin Massif, Oman Ophiolite; Major and
 713 Trace Element Geochemistry, and Os Isotope and PGE Systematics. *Journal of Petrology*,
 714 51(1–2), 201–227. <https://doi.org/10.1093/petrology/egp077>
- 715 Hansen, L. D., Dipple, G. M., Gordon, T. M., & Kellett, D. a. (2005). Carbonated Serpentinite
 716 (Listwanite) At Atlin, British Columbia: a Geological Analogue To Carbon Dioxide
 717 Sequestration. *The Canadian Mineralogist*, 43(1), 225–239.
 718 <https://doi.org/10.2113/gscanmin.43.1.225>
- 719 Hofmann, A. W. (2013). *Sampling Mantle Heterogeneity through Oceanic Basalts: Isotopes and
 720 Trace Elements. Treatise on Geochemistry: Second Edition* (2nd ed., Vol. 3). Elsevier Ltd.
 721 <https://doi.org/10.1016/B978-0-08-095975-7.00203-5>
- 722 Horita, J. (2014). Oxygen and carbon isotope fractionation in the system dolomite-water-CO₂ to
 723 elevated temperatures. *Geochimica et Cosmochimica Acta*, 129, 111–124.
 724 <https://doi.org/10.1016/j.gca.2013.12.027>
- 725 Hyndman, R. D., & Peacock, S. M. (2003). Serpentinization of the forearc mantle. *Earth and
 726 Planetary Science Letters*, 212(3–4), 417–432. <https://doi.org/10.1016/S0012->

- 727 821X(03)00263-2
- 728 Kamiya, S., & Kobayashi, Y. (2000). Seismological evidence for the existence of serpentinized
729 wedge mantle. *Geophysical Research Letters*, 27(6), 819–822.
730 <https://doi.org/10.1029/1999GL011080>
- 731 Kelemen, P. B., & Manning, C. E. (2015). Reevaluating carbon fluxes in subduction zones, what
732 goes down, mostly comes up. *Proceedings of the National Academy of Sciences*, 112(30),
733 E3997–E4006. <https://doi.org/10.1073/pnas.1507889112>
- 734 Kelemen, P. B., & Matter, J. M. (2008). In situ carbonation of peridotite for CO₂ storage.
735 *Proceedings of the National Academy of Sciences*, 105(45), 17295–17300.
736 <https://doi.org/10.1073/pnas.0805794105>
- 737 Kelemen, P. B., Matter, J. M., Streit, E. E., Rudge, J. F., Curry, W. B., & Blusztajn, J. (2011).
738 Rates and Mechanisms of Mineral Carbonation in Peridotite: Natural Processes and Recipes
739 for Enhanced, in situ CO₂ Capture and Storage. *Annual Review of Earth and Planetary
740 Sciences*, 39(1), 545–576. <https://doi.org/10.1146/annurev-earth-092010-152509>
- 741 Kelemen, P. B., Matter, J. M., Teagle, D. A. H., & Coggon, J. A. (Eds.). (2020). *Proceedings of
742 the Oman Drilling Project* (Vol. Phase 1 an). International Ocean Discovery Program.
743 <https://doi.org/10.14379/OmanDP.proc.2020>
- 744 Kelemen, P. B., Matter, J. M., Teagle, D. A. H., Coggon, J. A., & The Oman Drilling Project
745 Science. (2020). Site BT1: fluid and mass exchange on a subduction zone plate boundary.
746 In P. B. Kelemen, J. M. Matter, D. A. H. Teagle, J. A. Coggon, & et al. (Eds.), *Proceedings
747 of the Oman Drilling Project*. College Station, TX: International Ocean Discovery Program.
- 748 Kelemen, P. B., de Obeso, J. C., Leong, J. A. M., Godard, M., Okazaki, K., Kotowski, A. J., et
749 al. (2021). Mass transfer into the leading edge of the mantle wedge: Initial results from
750 Oman Drilling Project Hole BT1B. *Earth and Space Science Open Archive*.
751 <https://doi.org/10.1002/essoar.10507370.1>
- 752 Kerrick, D. M., & Connolly, J. A. D. (2001). Metamorphic devolatilization of subducted marine
753 sediments and the transport of volatiles into the Earth's mantle. *Nature*, 411, 293.
754 Retrieved from <http://dx.doi.org/10.1038/35077056>
- 755 Khedr, M. Z., Arai, S., Python, M., & Tamura, A. (2014). Chemical variations of abyssal
756 peridotites in the central Oman ophiolite: Evidence of oceanic mantle heterogeneity.
757 *Gondwana Research*, 25(3), 1242–1262. <https://doi.org/10.1016/J.GR.2013.05.010>
- 758 Klein, F., Humphris, S. E., & Bach, W. (2020). Brucite formation and dissolution in oceanic
759 serpentinite. *Geochemical Perspectives Letters*, 1–5.
760 <https://doi.org/10.7185/geochemlet.2035>
- 761 Kotowski, A. J., Cloos, M., Stockli, D. F., & Orent, E. B. (2021). Structural and thermal
762 evolution of an infant subduction shear zone: Insights from sub-ophiolite metamorphic
763 rocks recovered from Oman Drilling Project Site BT-1B. *Earth and Space Science Open
764 Archive*. <https://doi.org/https://doi.org/10.1002/essoar.10505943.1>
- 765 Lanphere, M. A., Coleman, R. G., & Hopson, C. A. (1981). Sr isotopic tracer study of the Samail
766 Ophiolite, Oman. *Journal of Geophysical Research: Solid Earth*, 86(B4), 2709–2720.
767 <https://doi.org/10.1029/JB086iB04p02709>

- 768 Macdonald, A. H., & Fyfe, W. S. (1985). Rate of serpentinization in seafloor environments.
769 *Tectonophysics*, 116(1–2), 123–135. [https://doi.org/10.1016/0040-1951\(85\)90225-2](https://doi.org/10.1016/0040-1951(85)90225-2)
- 770 McCulloch, M. T., Gregory, R. T., Wasserburg, G. J., & Taylor, H. P. (1981). Sm-Nd, Rb-Sr,
771 and ¹⁸O/¹⁶O isotopic systematics in an oceanic crustal section: evidence from the Samail
772 ophiolite. *Journal of Geophysical Research*, 86(B4), 2721–2735.
773 <https://doi.org/10.1029/JB086iB04p02721>
- 774 Menzel, M. D., Garrido, C. J., López Sánchez-Vizcaíno, V., Marchesi, C., Hidas, K., Escayola,
775 M. P., & Delgado Huertas, A. (2018). Carbonation of mantle peridotite by CO₂-rich fluids:
776 the formation of listvenites in the Advocate ophiolite complex (Newfoundland, Canada).
777 *Lithos*, 323, 238–261. <https://doi.org/10.1016/J.LITHOS.2018.06.001>
- 778 Menzel, M. D., Urai, J. L., de Obeso, J. C., Kotowski, A., Manning, C. E., Kelemen, P. B., et al.
779 (2020). Brittle Deformation of Carbonated Peridotite—Insights From Listvenites of the
780 Samail Ophiolite (Oman Drilling Project Hole BT1B). *Journal of Geophysical Research:*
781 *Solid Earth*, 125(10). <https://doi.org/10.1029/2020JB020199>
- 782 Monnier, C., Girardeau, J., Le Mée, L., & Polvé, M. (2006). Along-ridge petrological
783 segmentation of the mantle in the Oman ophiolite. *Geochemistry, Geophysics, Geosystems*,
784 7(11), n/a-n/a. <https://doi.org/10.1029/2006GC001320>
- 785 Nasir, S., Al Sayigh, A. R., Al Harthy, A., Al-Khirbash, S., Al-Jaaidi, O., Musllam, A., et al.
786 (2007). Mineralogical and geochemical characterization of listwaenite from the Semail
787 Ophiolite, Oman. *Chemie Der Erde - Geochemistry*, 67(3), 213–228.
788 <https://doi.org/10.1016/j.chemer.2005.01.003>
- 789 Noël, J., Godard, M., Oliot, E., Martinez, I., Williams, M., Boudier, F., et al. (2018). Evidence of
790 polygenetic carbon trapping in the Oman Ophiolite: Petro-structural, geochemical, and
791 carbon and oxygen isotope study of the Wadi Dima harzburgite-hosted carbonates (Wadi
792 Tayin massif, Sultanate of Oman). *Lithos*, 323, 218–237.
793 <https://doi.org/10.1016/J.LITHOS.2018.08.020>
- 794 de Obeso, J. C., & Kelemen, P. B. (2018). Fluid rock interactions on residual mantle peridotites
795 overlain by shallow oceanic limestones: Insights from Wadi Fins, Sultanate of Oman.
796 *Chemical Geology*. <https://doi.org/10.1016/J.CHEMGEO.2018.09.022>
- 797 de Obeso, J. C., & Kelemen, P. B. (2020). Major element mobility during serpentinization,
798 oxidation and weathering of mantle peridotite at low temperatures. *Philosophical*
799 *Transactions. Series A, Mathematical, Physical, and Engineering Sciences*, 378(2165),
800 20180433. <https://doi.org/10.1098/rsta.2018.0433>
- 801 de Obeso, J. C., Santiago Ramos, D. P., Higgins, J. A., & Kelemen, P. B. (2021). A Mg Isotopic
802 Perspective on the Mobility of Magnesium During Serpentinization and Carbonation of the
803 Oman Ophiolite. *Journal of Geophysical Research: Solid Earth*, 126(2), 1–17.
804 <https://doi.org/10.1029/2020JB020237>
- 805 Paulick, H., Bach, W., Godard, M., De Hoog, J. C. M., Suhr, G., & Harvey, J. (2006).
806 Geochemistry of abyssal peridotites (Mid-Atlantic Ridge, 15°20'N, ODP Leg 209):
807 Implications for fluid/rock interaction in slow spreading environments. *Chemical Geology*,
808 234(3–4), 179–210. <https://doi.org/10.1016/j.chemgeo.2006.04.011>
- 809 Prigent, C., Agard, P., Guillot, S., Godard, M., & Dubacq, B. (2018). Mantle Wedge

- 810 (De)formation During Subduction Infancy: Evidence from the Base of the Semail Ophiolitic
811 Mantle. *Journal of Petrology*, 59(11), 2061–2092. <https://doi.org/10.1093/petrology/egy090>
- 812 Quesnel, B., Boulvais, P., Gautier, P., Cathelineau, M., John, C. M., Dierick, M., et al. (2016).
813 Paired stable isotopes (O, C) and clumped isotope thermometry of magnesite and silica
814 veins in the New Caledonia Peridotite Nappe. *Geochimica et Cosmochimica Acta*, 183,
815 234–249. <https://doi.org/10.1016/j.gca.2016.03.021>
- 816 Rioux, M., Bowring, S., Kelemen, P. B., Gordon, S., Miller, R., & Dudás, F. (2013). Tectonic
817 development of the Semail ophiolite: High-precision U-Pb zircon geochronology and Sm-
818 Nd isotopic constraints on crustal growth and emplacement. *Journal of Geophysical*
819 *Research: Solid Earth*, 118(5), 2085–2101. <https://doi.org/10.1002/jgrb.50139>
- 820 Rioux, M., Garber, J., Bauer, A., Bowring, S., Searle, M. P., Kelemen, P. B., & Hacker, B.
821 (2016). *Synchronous formation of the metamorphic sole and igneous crust of the Semail*
822 *ophiolite: New constraints on the tectonic evolution during ophiolite formation from high-*
823 *precision U–Pb zircon geochronology*. *Earth and Planetary Science Letters* (Vol. 451).
824 <https://doi.org/10.1016/j.epsl.2016.06.051>
- 825 Schwarzenbach, E. M., Früh-Green, G. L., Bernasconi, S. M., Alt, J. C., & Plas, A. (2013).
826 Serpentinization and carbon sequestration: A study of two ancient peridotite-hosted
827 hydrothermal systems. *Chemical Geology*, 351, 115–133.
828 <https://doi.org/10.1016/j.chemgeo.2013.05.016>
- 829 Schwarzenbach, E. M., Gill, B. C., Gazel, E., & Madrigal, P. (2016). Sulfur and carbon
830 geochemistry of the Santa Elena peridotites: Comparing oceanic and continental processes
831 during peridotite alteration. *Lithos*. <https://doi.org/10.1016/j.lithos.2016.02.017>
- 832 Searle, M. P., & Cox, J. (2002). Subduction zone metamorphism during formation and
833 emplacement of the Semail ophiolite in the Oman Mountains. *Geological Magazine*, 139(3),
834 241–255. <https://doi.org/10.1017/S0016756802006532>
- 835 Searle, M. P., & Malpas, J. (1980). Structure and metamorphism of rocks beneath the Semail
836 ophiolite of Oman and their significance in ophiolite obduction. *Transactions of the Royal*
837 *Society of Edinburgh: Earth Sciences*, 71(4), 247–262.
838 <https://doi.org/10.1017/S0263593300013614>
- 839 Searle, M. P., Waters, D. J., Martin, H. N., & Rex, D. C. (1994). Structure and metamorphism of
840 blueschist-eclogite facies rocks from the northeastern Oman Mountains. *Journal -*
841 *Geological Society (London)*, 151(3), 555–576. <https://doi.org/10.1144/gsjgs.151.3.0555>
- 842 Soret, M., Agard, P., Dubacq, B., Plunder, A., & Yamato, P. (2017). Petrological evidence for
843 stepwise accretion of metamorphic soles during subduction infancy (Semail ophiolite,
844 Oman and UAE). *Journal of Metamorphic Geology*, 35(9), 1051–1080.
845 <https://doi.org/10.1111/jmg.12267>
- 846 Stanger, G. (1985). Silicified serpentinite in the Semail nappe of Oman. *Lithos*, 18, 13–22.
847 [https://doi.org/10.1016/0024-4937\(85\)90003-9](https://doi.org/10.1016/0024-4937(85)90003-9)
- 848 Stewart, E. M., & Ague, J. J. (2020). Pervasive subduction zone devolatilization recycles CO₂
849 into the forearc. *Nature Communications*, 11(1), 1–8. [https://doi.org/10.1038/s41467-020-](https://doi.org/10.1038/s41467-020-19993-2)
850 [19993-2](https://doi.org/10.1038/s41467-020-19993-2)

- 851 Tibi, R., Wiens, D. A., & Yuan, X. (2008). Seismic evidence for widespread serpentized
852 forearc mantle along the Mariana convergence margin. *Geophysical Research Letters*,
853 35(13), 267–270. <https://doi.org/10.1029/2008GL034163>
- 854 Tsuji, Y., Nakajima, J., & Hasegawa, A. (2008). Tomographic evidence for hydrated oceanic
855 crust of the Pacific slab beneath northeastern Japan: Implications for water transportation in
856 subduction zones. *Geophysical Research Letters*, 35(14), 1–5.
857 <https://doi.org/10.1029/2008GL034461>
- 858 Villey, M., Le Metour, J., & de Gramont, X. (1986). Geological Map of Fanjah. Muscat, Oman:
859 Ministry of Petroleum and Minerals, Directorate General of Minerals. Sultanate of Oman.
- 860 Weis, D., Kieffer, B., Maerschalk, C., Barling, J., De Jong, J., Williams, G. A., et al. (2006).
861 High-precision isotopic characterization of USGS reference materials by TIMS and MC-
862 ICP-MS. *Geochemistry, Geophysics, Geosystems*, 7(8).
863 <https://doi.org/10.1029/2006GC001283>
- 864 Weyhenmeyer, C. E. (2000). *Origin and evolution of groundwater in the alluvial aquifer of the*
865 *Eastern Batinah Coastal Plain, Sultanate of Oman : a hydrogeochemical approach*. PhD
866 Thesis, Universität Bern, Bern, Switzerland.
- 867 Wilde, A., Simpson, L., & Hanna, S. (2002). Preliminary study of tertiary hydrothermal
868 alteration and platinum deposition in the Oman ophiolite. *Journal of the Virtual Explorer*, 6,
869 7–13.
- 870 Yoshikawa, M., Python, M., Tamura, A., Arai, S., Takazawa, E., Shibata, T., et al. (2015). Melt
871 extraction and metasomatism recorded in basal peridotites above the metamorphic sole of
872 the northern Fizz massif, Oman ophiolite. *Tectonophysics*, 650, 53–64.
873 <https://doi.org/10.1016/j.tecto.2014.12.004>
- 874 Zeko, D. (2021). *Carbonation of the Oman ophiolite during subduction and emplacement*.
875 University of British Columbia.
- 876